

MODELING AND DESIGN OF A BI-STABLE SPRING
MECHANISM

By

BRIAN DAVID LAFERRIERE

A project report submitted in partial fulfillment of
the requirements for the degree of

MASTER OF SCIENCE IN MECHANICAL ENGINEERING

WASHINGTON STATE UNIVERSITY
School of Mechanical and Materials Engineering

MAY 2017

ACKNOWLEDGMENT

I would like to thank my advisor Dr. John Swensen for his help on this project and I would also like to thank Carson Schlect for his preliminary work done on the force and potential energy characterization/representation of single springs.

MODELING AND DESIGN OF A BI-STABLE SPRING MECHANISM

Abstract

by Brian David LaFerriere, M.S.
Washington State University
May 2017

Chair: John P. Swensen

The ability to change stiffness is a capability exhibited through the animal kingdom, with many recent advances in tunable stiffness in the area of robotics. This report describes and demonstrates a mechanism design that provides the ability to make modular subcomponents with tunable stiffness by creating a bi-stable mechanism that exhibits different stiffnesses in each of the stable configurations. The design is based on controlled buckling of two linear springs in series and allows design-time control over the stiffnesses, equilibrium points, and energy required to transition between the stable configurations. A prototype mechanism was designed and experimental data was obtained. This project demonstrates the bi-stably and tunability of the buckling spring mechanism.

TABLE OF CONTENTS

	Page
ACKNOWLEDGMENTS	ii
ABSTRACT.....	iii
LIST OF TABLES	v
LIST OF FIGURES	vi
CHAPTER	
CHAPTER ONE: INTRODUCTION.....	1
CHAPTER TWO: ANALYSIS OF SPRING BUCKLING	5
CHAPTER THREE: OPTIMIZATION OF THE SERIES SPRING BI-STABLE MECHANISM	12
CHAPTER FOUR: PROTOTYPE MECHANISM.....	16
CHAPTER FIVE: EXPERIMENTAL DATA.....	18
CHAPTER SIX: CONCLUSION	26
REFERENCES	27

LIST OF TABLES

	Page
Table 1.1: Variables	9
Table 5.1: Properties of 3 Springs.....	19

LIST OF FIGURES

	Page
Figure 1.1: Bi-stable Mechanism with Adjustable Points	2
Figure 2.1: Test Apparatus.....	5
Figure 2.2: Compression and Buckling of a Spring at 5 controlled Points.....	6
Figure 2.3: Four regions of spring compression and buckling	7
Figure 2.4: Bi-stable liner spring mechanism	9
Figure 3.1: Surface Plot of Potential Energy	12
Figure 3.2: Potential Energy vs. Displacement.....	13
Figure 3.3: Potential Energy vs a for various values of b	14
Figure 4.1: Initial Prototype Design and Construction	16
Figure 4.2: Apparatus for Force Measurements	17
Figure 5.1: Spring Properties Test Setup	18
Figure 5.2: Force vs. Displacement at $a = 15\text{mm}$	20
Figure 5.3: Force/Displacement curves with $b = 6\text{mm}$	21
Figure 5.4: Experimental Data Overlaid	22
Figure 5.5: High Stiffness Spring A with Medium Stiffness Spring B	24
Figure 5.6: Low Stiffness Spring A and High Stiffness Spring B	24
Figure 5.7: Low Stiffness Spring A and Medium Stiffness Spring B	25

CHAPTER ONE: INTRODUCTION

Traditionally, robotic systems have followed the paradigm of being comprised primarily of rigid structures with relatively few degrees of freedom and well-characterized motion driven by actuators directly connected to the rigid links. In recent years, there has been an explosion of research in the area of compliant and soft robotics, as they provide the promise of allowing robots and humans to work and collaborate in the same workspace. However, compliant devices inherently limit the ability to exert forces and interact with their surroundings because of their compliant nature. In the case of soft robotics, this results in both actuators and systems that are primarily concerned with the problem of compliance matching to the task of the robotic system [1]. Hence, there is a great need for materials and mechanisms that have the ability to dynamically change between acting as a soft or a rigid robotic component.

This paper presents a general two-spring design for achieving a bi-stable, compliant mechanism where the stiffness exhibited in each of the stable configurations can be selected at design-time. In contrast to many other mechanisms that are either tunably-compliant or bi-stable, the proposed approach is both compliant and bi-stable and provides greater ability to tune the design by allowing the designer to prescribe the locations of the stable equilibria, the quasi-linear stiffness in each of the equilibria, and the amount of energy required to transition between the equilibria. A prototype of the mechanism is shown in Figure 1.1(Top) and the tunability is described in

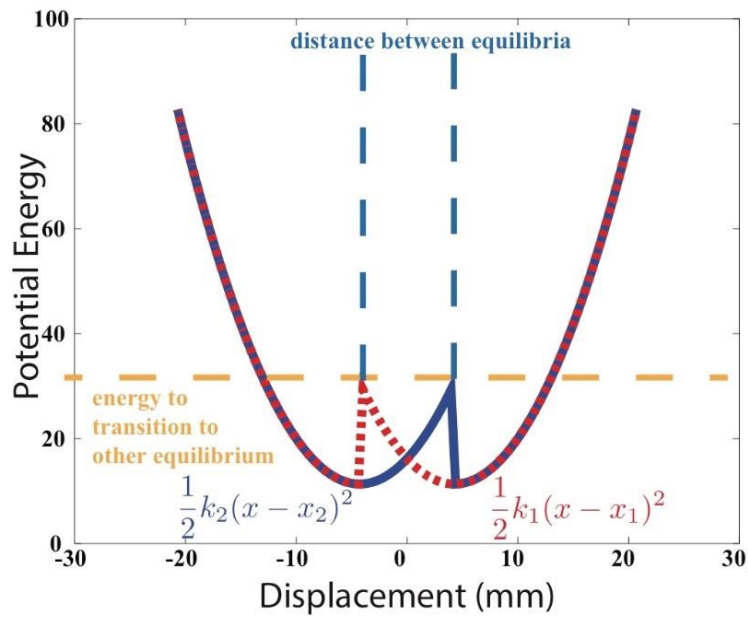
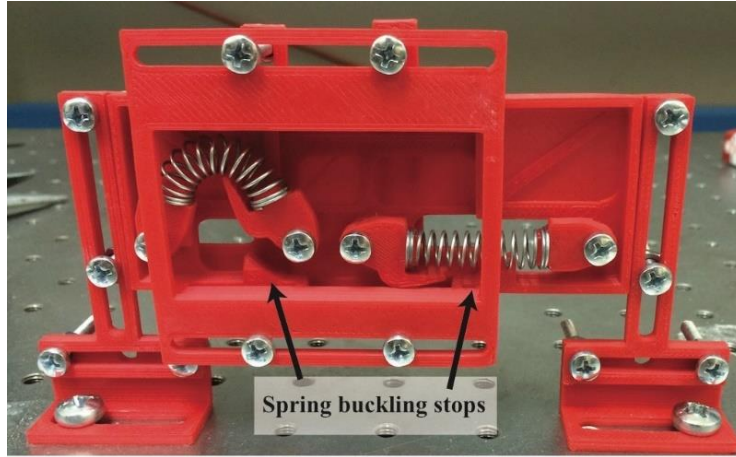


Figure 1.1: Bi-stable mechanism with adjustable equilibrium points. The stiffness in each of the stable configurations can be defined by the selection of each of the series springs. Transition between the stable configurations requires the application of an external force (not shown).

Figure 1.1(Bottom) where both the prototype mechanism is shown as well as the effects of each design parameter on the potential energy profile of the mechanism.

Tunable stiffness in robotics:

Variable stiffness actuators

Many variable stiffness actuators require complex design and machining to achieve a change of stiffness in even a single degree of freedom [2]–[4]. These often involve a high degree of complexity in terms of motors, mechanisms, and/or cable routings. Other approaches require high bandwidth feedback control to render a variable stiffness through a control system [5], [6]. These approaches are usually not scalable and are more targeted at applications with a distinct drive train, rather than as material actuators and structures. However, when amenable these approaches provide the highest fidelity of rendered variable stiffness.

Variable stiffness structures

Tensile integrity, or tensegrity, structures were initially used in architecture and artwork, with the term coined by Buckminster Fuller. It is integrity of the whole. When applied to robotic systems, these tensegrity structures are designed such that the robot can selectively release tension in one or more cables, resulting in a predictable motion during collapse. Sequential loading and unloading of the cable generates reproducible gaits [7], [8]. Other researchers are focusing on the valid tensegrity configurations that result in predictable deformations and their associated control [9], [10].^[11]_{SEP}

Bi-stable mechanisms

Bi-stable mechanisms, particularly those using compliant flexure to define the stable equilibria of the mechanism, are a popular technique to passive compliance with multiple stable positions. The most common designs are variations of the straight-leg bi-stable mechanism (SLBM) [11]–[14], with many computational models and simplifications to treat small flexures using more simple kinematics [15]–[18]. Many of these designs have been further developed

with regards to specific manufacturing processes and device capabilities, such as stamp fabrication, use in medical devices, and deriving k-stable mechanism through the use of multiple bi-stable mechanisms [14], [19], [20]. The work presented in this paper combines the beneficial aspect of both tunably-compliant mechanisms and bi-stable mechanisms. It provides designers with the ability to control the stiffness in each of the equilibria, shape the potential energy to determine the external forces needed to transition between equilibria, and to determine the relative location of the equilibria with respect to each other. Chapter Two describes the methods for designing and analyzing a single-spring and double-spring controlled buckling mechanism. Chapter Three provides methods for analyzing and optimizing the geometry of the springs and overall mechanism length to maximize the distance between equilibria and maximizing the energy required to transition between equilibria. Chapter 4 shows the first prototypes of the device. Finally, Chapter 5 shows experimental results from one of the prototype mechanisms.

CHAPTER TWO: ANALYSIS OF SPRING BUCKLING

Buckling-point Control of a Single Spring:

Initial tests of spring compression and buckling were performed using the apparatus shown in Figure 2.1. The apparatus was designed to be able to control the buckling point of a single spring. The spring used for testing was made of 0.787mm diameter music wire (W.B. Jones Spring Co.). The spring ends were attached to pin joints. The left joint was attached to a load cell (Transducer Techniques MLP series) and the right joint was attached to a linear actuator (Firgelli Technologies' Miniature Linear Actuator). As the linear actuator moved to the left the spring was compressed applying force to the fixed load cell. The actuator was intentionally aligned slightly off center of the springs axis. Consequently, during compression, without any radial constraints, the spring naturally buckled downward at a very small displacement of about 3 mm. A lever arm was added to not only constrain the springs vertical motion but to force the spring to buckle upward. The lever arm rested horizontally and was constrained to only rotate in the clockwise direction. When the lever rotated, it forced the spring upward causing it to buckle. The rotation of the lever was triggered by a wedge attached to the head of the actuator hitting it as the actuator moved left. Changing the location of the lever

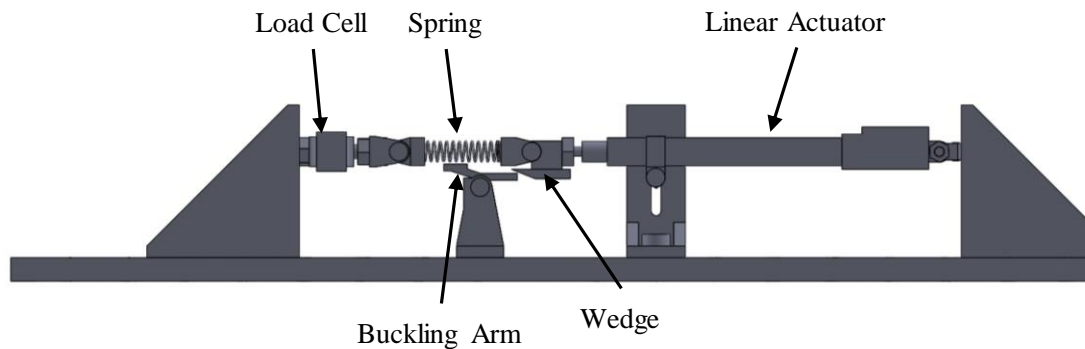


Figure 2.1: Test Apparatus

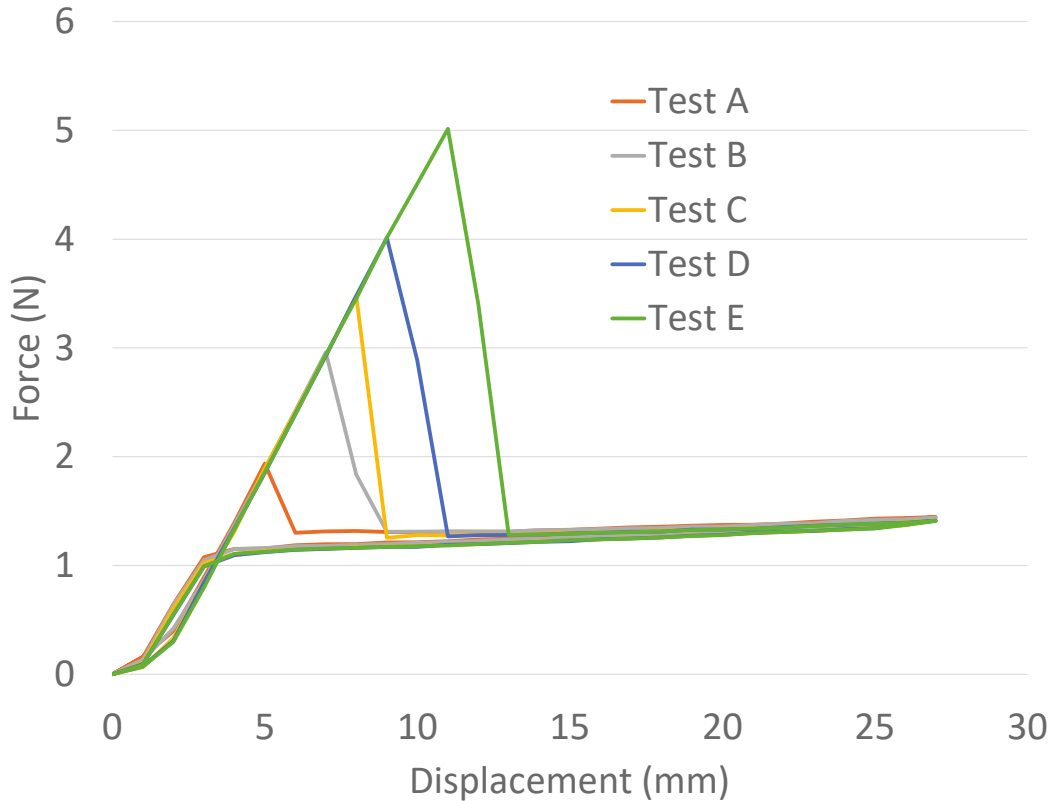


Figure 2.2: Compression and Buckling of a spring at 5 controlled points.

changed the buckling location of the spring. This made it possible to test the spring force at different points of buckling. Spring compression tests were performed at 5 different buckling points. Each test cycled the spring from its resting point to a compression distance of 27mm and then back to rest. All tests were performed four times. The average for each of the tests is plotted in Figure 2.2.

A typical compression/buckling cycle consisted of 4 different regions as shown in Figure 2.3. Region 1 is a normal spring compression curve that follows Hooke's law. When the spring buckles, the force drops off to Region 2 which is a nearly constant force. Region 3 is essentially the same as Region 2 except that it extends back along the x axis further. Region four is when the spring unbuckles and returns to its normal curve. The apparent small differences between the

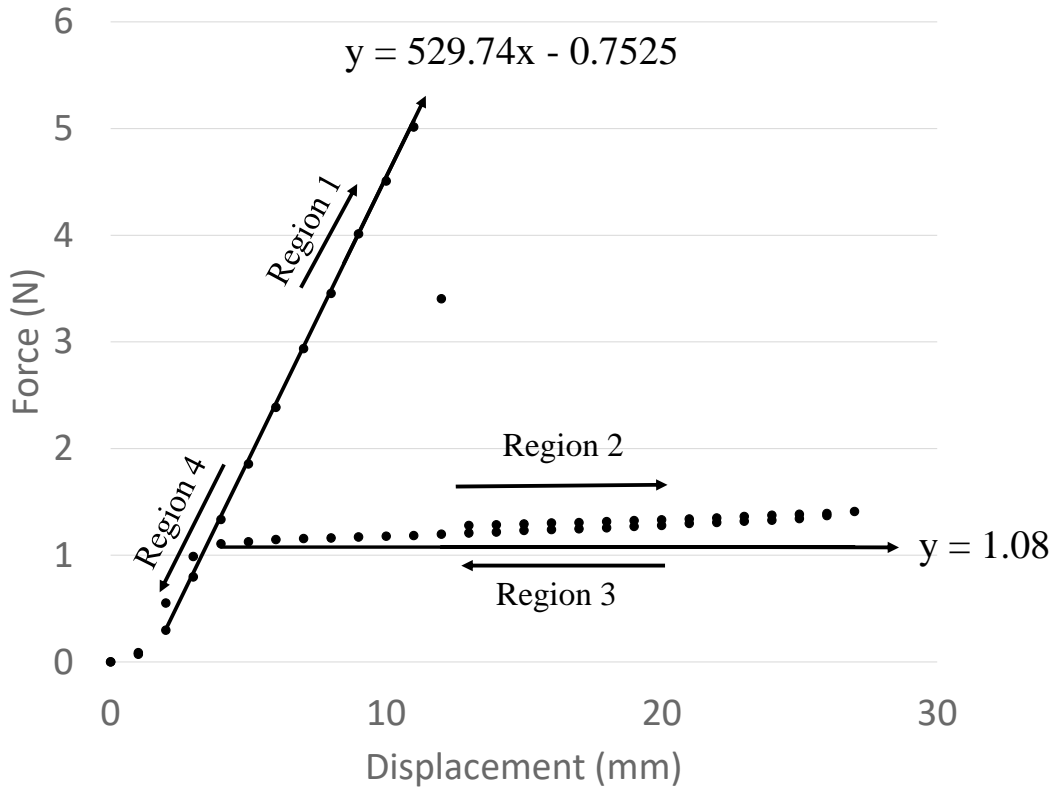


Figure 2.3. Four regions of spring compression and buckling and curve fit. compression and decompression regions are most likely not real and are probably due to slop in the linear actuator.

Because the test setup only controls the buckling point of the spring, the unbuckling point is always at the same natural unbuckling point. Because of this, one piecewise equation (1) is required to describe the compression and buckling and another is required to describe the decompression and unbuckling (2). The force exerted by the buckled spring can be described as a constant force, c .

$$(1) F_{com.}(x) = \begin{cases} c, & x_{min} \leq x < x_b \\ -kx, & x_b \leq x \leq 0 \end{cases}$$

$$(2) F_{decom.}(x) = \begin{cases} c, & x_{min} \leq x < x_u \\ -kx, & x_u \leq x \leq 0 \end{cases}$$

where k is the spring constant, x_b is the buckling point of the spring as it is compressed, c is the near constant force applied by the buckled spring and x_u is the unbuckling point of the spring.

The potential energy of the spring during compression and decompression can also be described using two piecewise equations (3) and (4).

$$(3) \ U_{com.}(x) = \begin{cases} (x_u - x)c + \frac{1}{2}kx_u^2, & x_{min} \leq x < x_b \\ \frac{1}{2}kx^2, & x_b \leq x \leq 0 \end{cases}$$

$$(4) \ U_{decom.}(x) = \begin{cases} (x_u - x)c + \frac{1}{2}kx_u^2, & x_{min} \leq x < x_u \\ \frac{1}{2}kx^2, & x_u \leq x \leq 0 \end{cases}$$

Equilibrium of Series Spring Mechanism:

These equations were then used to develop a model for a mechanism composed of two springs arranged in series. A basic schematic of this setup is shown in Figure 2.4. To simplify this model two identical springs were used. The two ends of the springs were attached to pin joints that were fixed in place and the center connection was able to move freely along the horizontal axis. The initial amount of compression on the springs is described using variable a . Given a linear mechanism with two springs, each with a rest length of L_0 a pre-compression of a would cause an initial load length, L_i (5). The maximum compression distance of the spring is also dependent on a as shown in (6)

$$(5) \ L_i = L_0 - a$$

$$(6) \ x_{max} = L_{max} - a$$

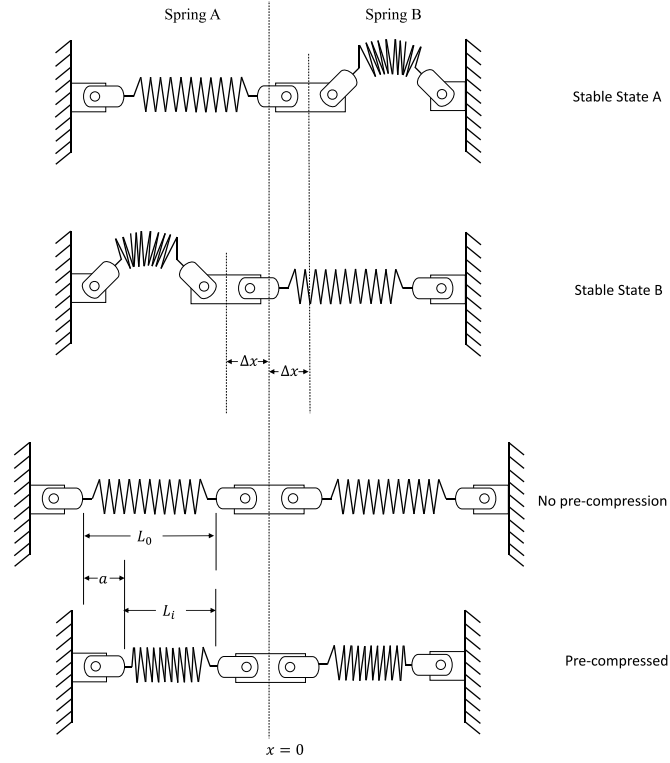


Figure 2.4: Bi-stable linear spring mechanism.

Displacement of the mechanism is measured relative to the center of the system. The goal was to obtain a spring mechanism with two stable states. One state (State A) would have spring A buckled with spring B unbuckled. The other state (State B) would have spring B buckled while

Table 1.1: Variables.

Variable	Description
L_{max}	Maximum Compression Length of Spring
L_0	Rest Length of Spring
a	Pre-compression distance
x_{max}	Maximum displacement of system
x_{min}	Minimum displacement of system
C	Force Applied by Buckled Spring
k	Spring Constant
b	Relative Buckling Point of Spring ($b = x_b - a$)
b'	Relative Unbuckling Point of Spring ($b' = x_u - a$)

spring A is unbuckled. To fully describe the force and potential energy of the model, different sets of equations are required. To describe the forces exerted when the mechanism moves from Mode 1 to Mode 2 equations (7) and (8) are used. (7) describes the force exerted by spring A starting from a buckled state all the way to it unbuckled state at the far right. Likewise, (8) describes the force exerted by spring B as it moves from an unbuckled state at the far left to its buckled state at the far right. Integrating these equations with respect to x gives the potential energy as described in (11) and (12). The desired equilibrium points (i.e., the stable positions at which one spring is buckled while the other is not) can be found graphically by plotting the total potential energy of the system (12). The variables in equations (7) through (12) are described in Table 1.1.

$$(7) F_{A_{L \rightarrow R}}(x) = \begin{cases} C, & x_{min} \leq x < -b' \\ -k(x - a), & -b' \leq x \leq x_{max} \end{cases}$$

$$(8) F_{B_{L \rightarrow R}}(x) = \begin{cases} -k(x + a), & x_{min} \leq x < b \\ -C, & b \leq x \leq x_{max} \end{cases}$$

$$(9) F_{Total_{L \rightarrow R}}(x) = F_{A_{L \rightarrow R}} + F_{B_{L \rightarrow R}}$$

$$(10) U_{A_{L \rightarrow R}}(x) = \begin{cases} C(-b' - x) + \frac{1}{2}k(b')^2, & x_{min} \leq x < -b' \\ \frac{1}{2}k(x - a)^2, & -b' \leq x \leq x_{max} \end{cases}$$

$$(11) U_{B_{L \rightarrow R}}(x) = \begin{cases} \frac{1}{2}k(x + a)^2, & -x_{min} \leq x < b \\ C(x - b') + \frac{1}{2}k(b')^2, & b \leq x \leq x_{max} \end{cases}$$

$$(12) U_{Total_{L \rightarrow R}}(x) = U_{A_{R \rightarrow L}} + U_{B_{R \rightarrow L}}$$

A similar set of equations, (8) through (13), can be used to describe the force and potential energy when the mechanism moves from right to left.

$$(13) F_{A_{R \rightarrow L}}(x) = \begin{cases} C, & x_{min} \leq x < -b \\ -k(x - a), & -b \leq x \leq x_{max} \end{cases}$$

$$(14) F_{B_{R \rightarrow L}}(x) = \begin{cases} -k(x + a), & x_{min} \leq x < b' \\ -C, & b' \leq x \leq x_{max} \end{cases}$$

$$(15) F_{Total_{R \rightarrow L}}(x) = F_{A_{R \rightarrow L}} + F_{B_{L \rightarrow R}}$$

$$(16) U_{A_{R \rightarrow L}}(x) = \begin{cases} C(-b' - x) + \frac{1}{2}k(b')^2, & x_{min} \leq x < -b \\ \frac{1}{2}k(x - a)^2, & -b \leq x \leq x_{max} \end{cases}$$

$$(17) U_{B_{R \rightarrow L}}(x) = \begin{cases} \frac{1}{2}k(x + a)^2, & x_{min} \leq x < b' \\ C(x - b') + \frac{1}{2}k(b')^2, & b' \leq x \leq x_{max} \end{cases}$$

$$(18) U_{Total_{R \rightarrow L}}(x) = U_{A_{L \rightarrow R}} + U_{B_{L \rightarrow R}}$$

CHAPTER THREE: OPTIMIZATION OF THE SERIES SPRING

BI-STABLE MECHANISM

Initial optimization of the multi-spring mechanism involved making a surface plot of equation (7) and equation (13) as shown in Figure 3.1(A). The spring pre-compression was varied from 0 to 14 mm. The buckling point (x_u) was fixed at 10.5 mm of spring compression. As can be seen, with an initial pre-compression of zero there is a single potential energy well as shown in Figure 3.1(B). As the pre-compression increases, two potential energy wells appear as shown in Figure 3.1(C)-(D). The buckling points of springs A and B are visible. The optimum

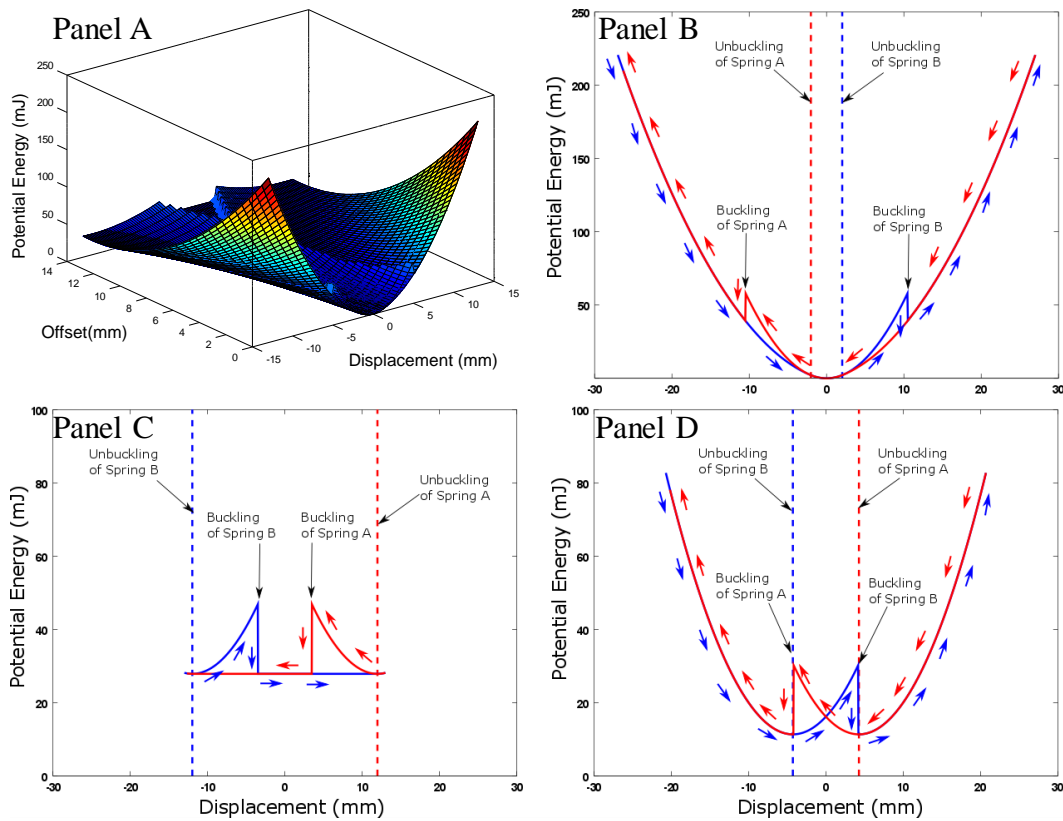


Figure 3.1: Surface Plot of Potential Energy (J) vs. Displacement. Panel A: Surface plot of potential energy vs displacement vs. pre-compression. Panels B, C & D: Slice of surface plot at pre-compression of 0 mm, 6.3mm and 14mm respectively.

pre-compression is at the most stable energy well. Figure 3.2 shows to the potential energy of the system when a is equal to 4mm and 8mm. It also shows the potential energy of a spring system without buckling (solid black curve). This intersects with the buckled curves in Figure 3.2(A) and shows that although there are two potential energy wells for buckling there is a third potential energy well for a state were both springs are unbuckled. This adds a level of instability that may not be desirable depending on the application. As a increases the amount of energy required to reach this state increases. Once a is large enough the double unbuckled state is no longer accessible as can be seen in Figure 3.2(B) but another state appears where both springs

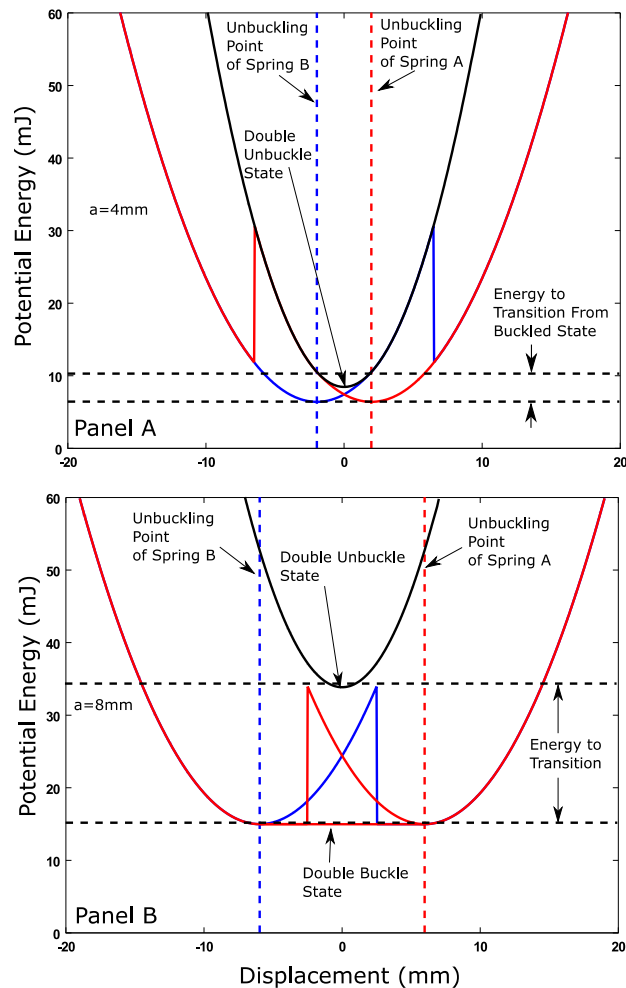


Figure 3.2: Potential Energy vs displacement for $a=4\text{mm}$ and $a=8\text{mm}$.

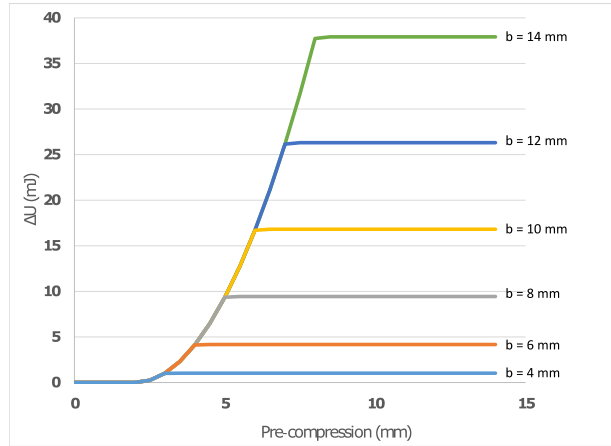


Figure 3.3. Potential Energy vs a for various values of b .

are buckled. To limit the system to only two states where either one spring is buckled or the other is buckled, the buckling point of the spring and the unbuckling point need to match. Figure 3.3 graphs the Energy to Transition (ΔU) vs a for various values of b . As can be seen, the amount of energy required increases and then plateaus. The plateau is reached when the unbuckled state is no longer available. Figure 3.3 shows that the Energy to Transition can be optimized by changing the pre-compression (a) and the controlled buckling point (b).

The mechanism design and the analysis tools given in Section II provide the ability to optimize:

- A) the location of the stable equilibrium
- B) the stiffness in each of the equilibrium (future work)
- C) the energy required to transition between the stable equilibrium.

These three properties are controlled by:

- I. The stiffness of the springs
- II. The buckling point of the spring as defined by the buckling-assist in the mechanism design
- III. The pre-compression of the two springs

This paper presents a manual optimization technique done through a visual analysis of the slices of the surface plot given in Figure 3.1(A), however future work will involve the co-optimization of all variables and automated mechanism design. This manual optimization was used to generate a prototype mechanism.

CHAPTER FOUR: PROTOTYPE MECHANISM

An initial prototype mechanism was designed and fabricated. The layout and construction are shown in Figure 4.1. The sides of the component mount on vertical channels attached to an optical bread board. The body of the component clamps around it like a clam shell and is free to move left and right. The pins on the joints were keyed to prevent downward buckling of the springs. The wedges at the bottom of the sides and on the center joints cause the springs to

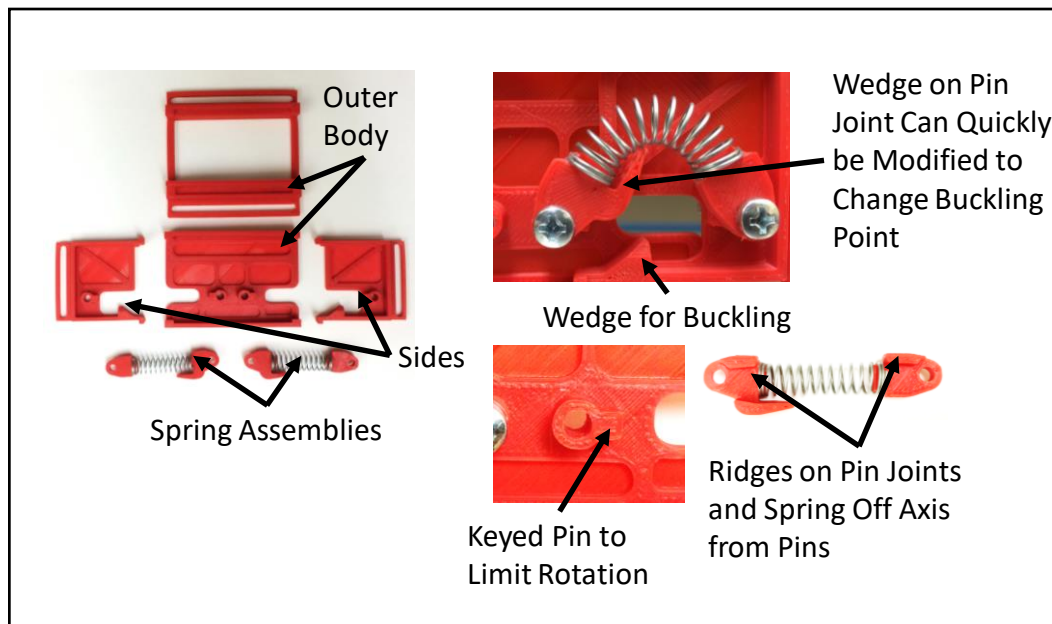
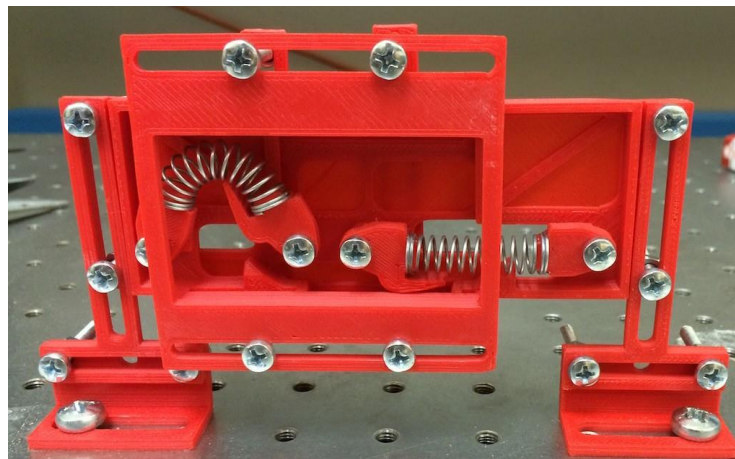


Figure 4.1: Initial Prototype Design and Construction.

buckle. The pre-compression can easily be changed by changing the mounting position of the sides on the bread board. The buckling point can be changed by changing the shape of the wedge on the center joints. The joints could easily be modified to accommodate different springs as well.

Although this initial prototype was a proof of concept, significant friction in the sliding mechanism made it less than ideal for measuring the forces in the series spring setup and the buckling point could not be easily changed without reprinting the pin joints. The apparatus was redesigned for adjustability as shown in Figure 4.2.

This setup made it possible to easily change both the buckling points and the pre-compression by turning the threaded rods which support the outer mounting joints and the buckling parts.

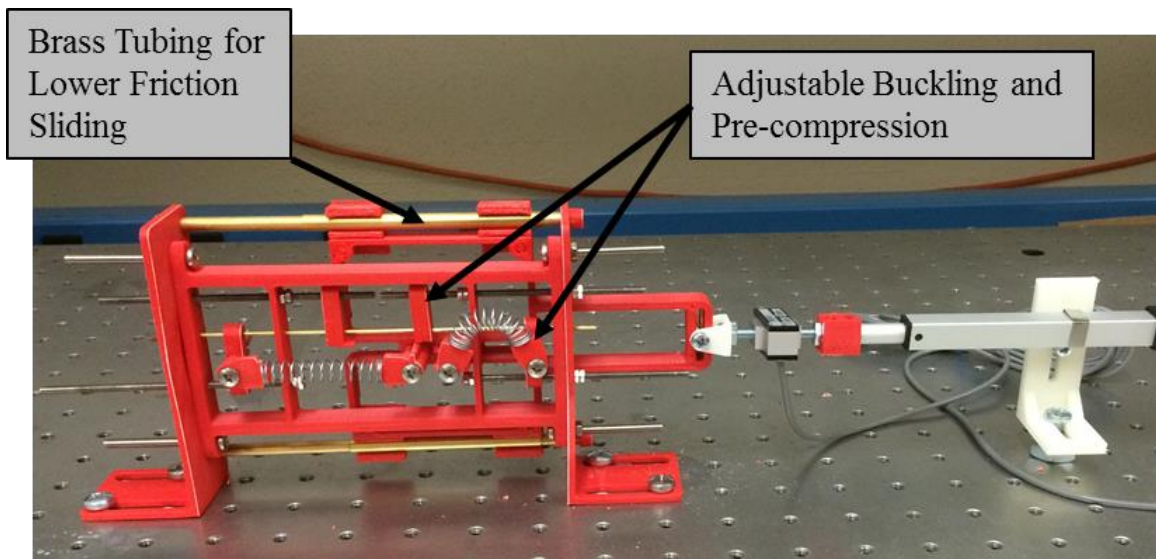


Figure 4.2: Apparatus for Force Measurements.

CHAPTER FIVE: EXPERIMENTAL DATA

Spring Selection and Properties:

Three springs with different stiffnesses were selected. Their properties were measured using the setup shown in Figure 5.1. The spring constant and the buckled force of the spring were both measured. The spring constant was obtained by measuring the force at a compression of 10mm. The constant buckling force was obtained by measuring the force of a buckled spring, under compression, every 1mm over a distance of 5mm. The average of these five measurements was taken as the buckled spring force. A summary of each of the three springs properties is shown in Table 5.1.

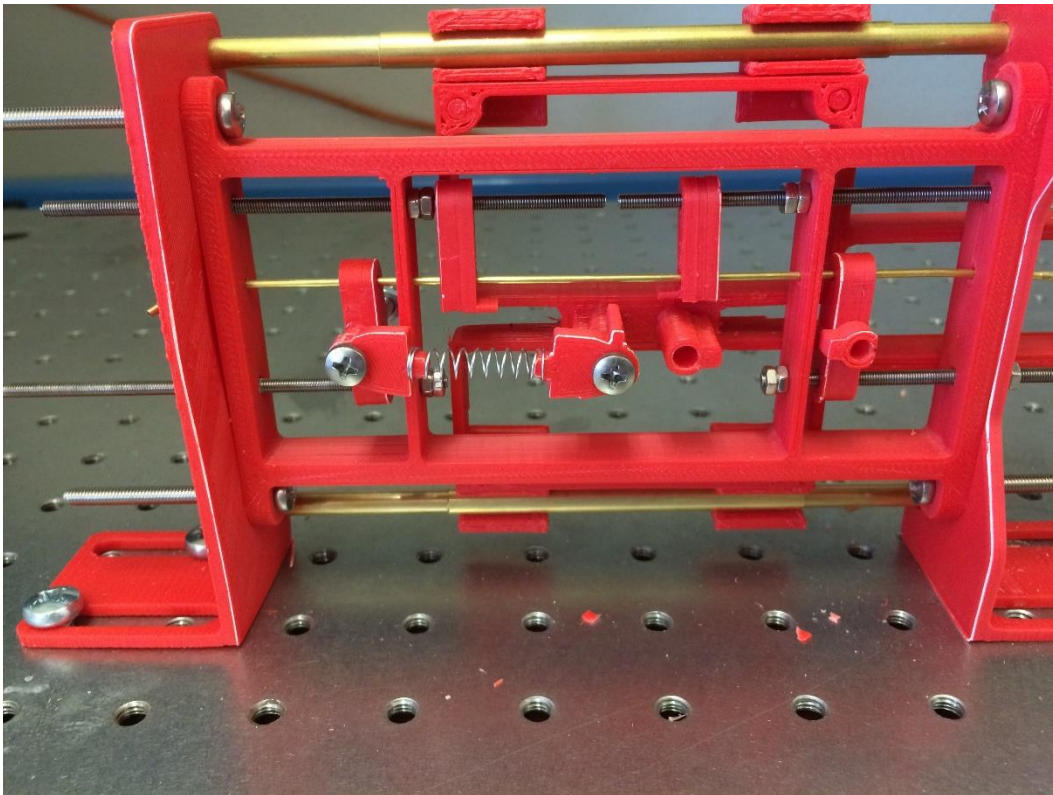





Figure 5.1: Spring Properties Test Setup.

Table 5.1: Properties of 3 Springs.

Medium Stiffness	High Stiffness	Low Stiffness
		
$k = 0.48 \text{ N/mm}$	$k = 0.64 \text{ N/mm}$	$k = 0.35 \text{ N/mm}$
$C = 1.5 \text{ N}$	$C = 2.1 \text{ N}$	$C = 0.50 \text{ N}$

Measurements of a Medium-Medium Setup:

Figure 5.2 shows the results from testing a mechanism consisting of two of the medium stiffness springs. The buckling point was varied while the pre-compression was held constant.

The two horizontal lines indicate the location of the equilibrium points for the mechanism. The equilibrium points are where the compressed force of one spring matches the buckled force of the other. These locations are circled. As is expected the equilibrium point does not change with the buckling point.

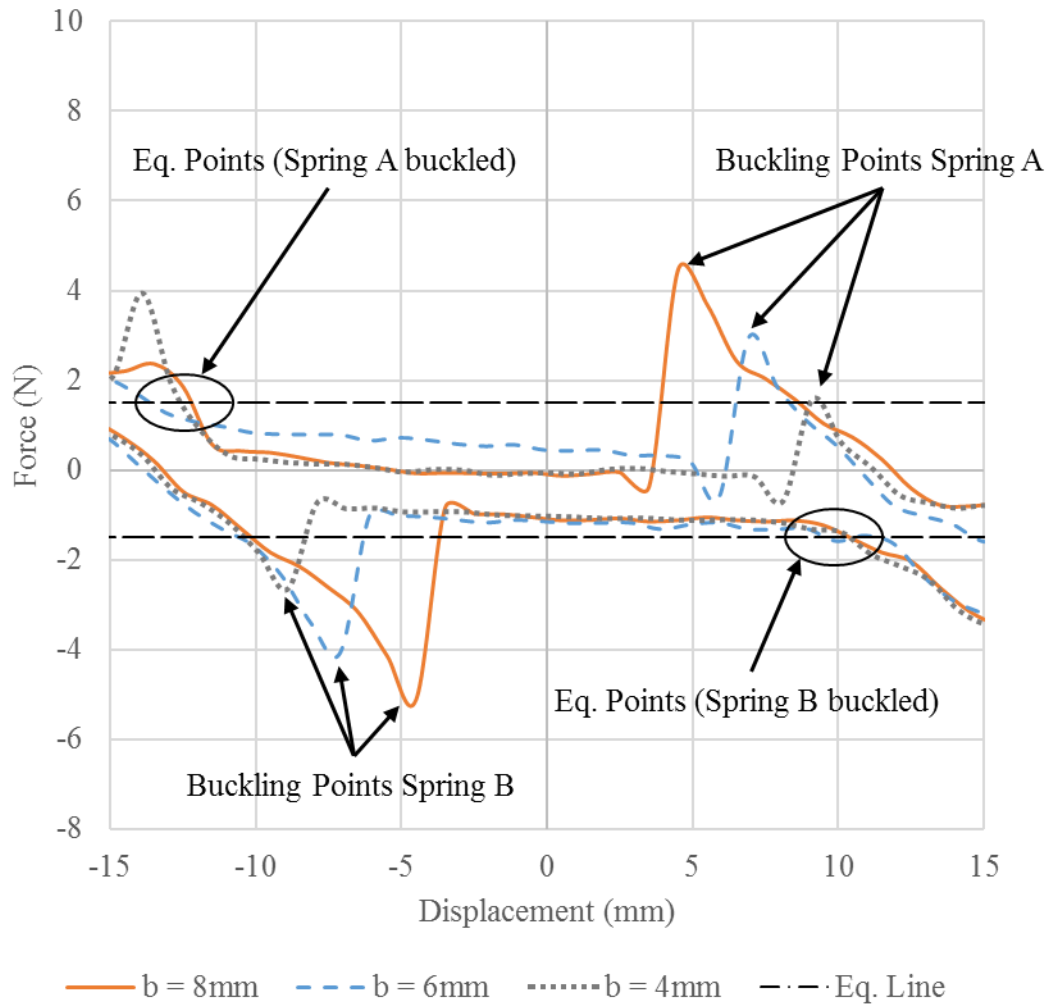


Figure 5.2: Force vs. Displacement at $a = 15\text{mm}$.

Likewise, tests were done with b held constant while changing the value for a as shown in Figure 5.3. This graph shows that holding the buckling point constant keeps the peak close to the same value but the equilibrium point changes since the overall movement of the springs changes with each value of a .

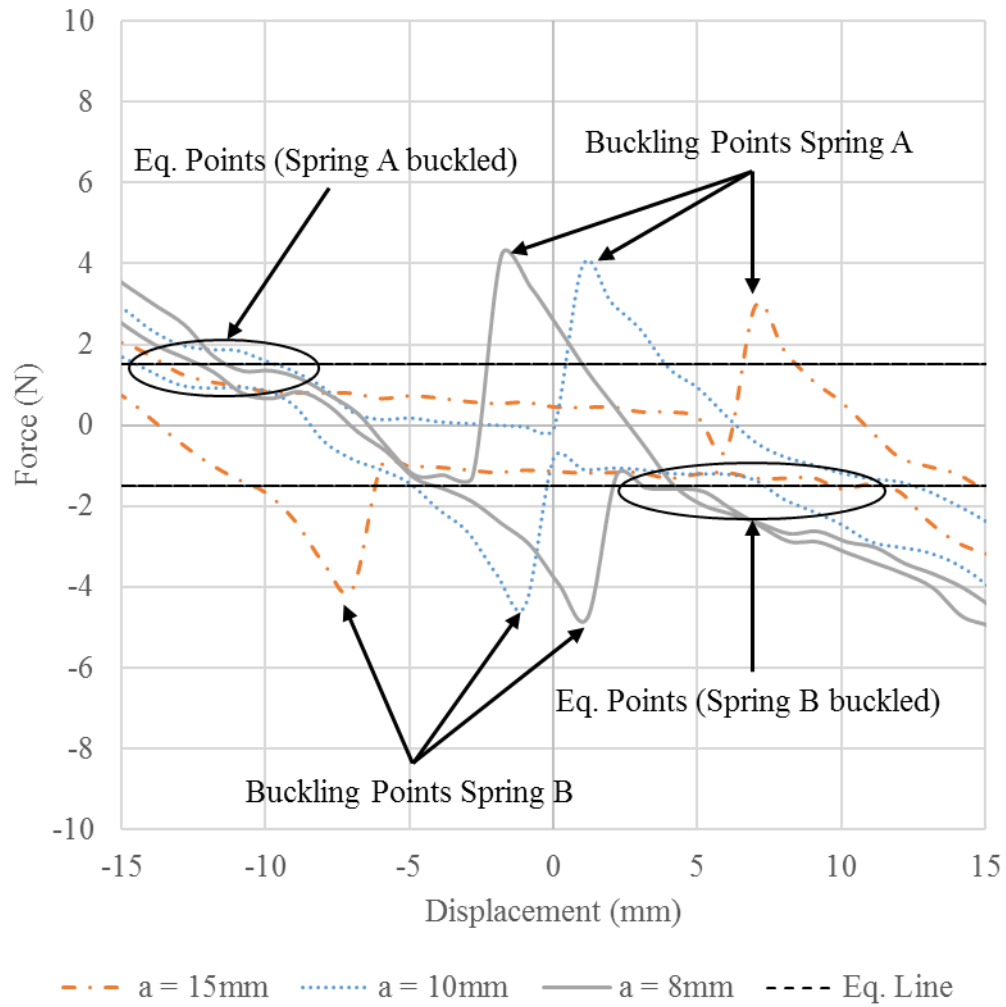


Figure 5.3: Force/Displacement curves with $b = 6\text{mm}$.

Comparison of Experimental Data to the Model:

Figure 5.4 shows the curve for $a = 10$ and $b = 6$ overlaid with the calculated model for this spring. As can be seen, the experimental data does not quite match with the model. The slopes of the curves are close but the peaks for the buckling are not. This could be due to a combination of any of the following factors:

- Slop in the linear actuator ($\pm 0.5\text{mm}$)
- Friction in the Mechanism
- Precision of setting the buckling point and pre-compression

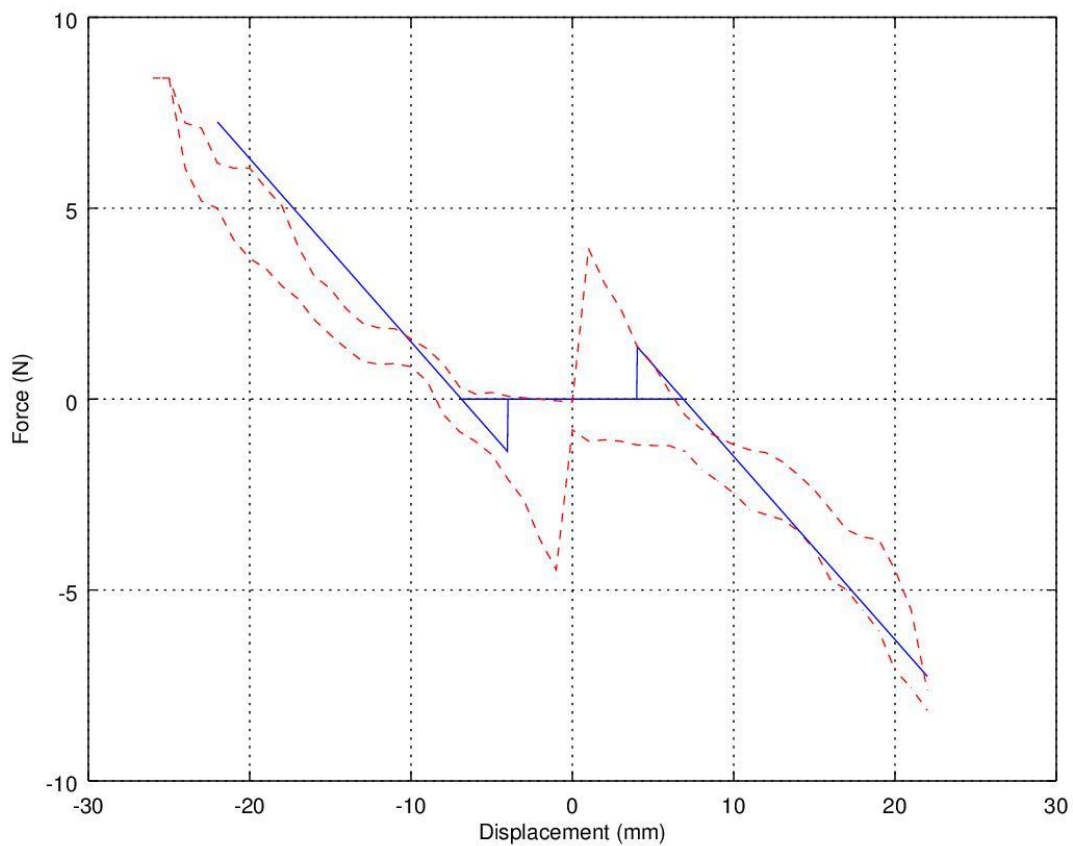


Figure 5.4: Experimental Data Overlaid on Calculated Model.

The most likely cause of the discrepancy is the slight intentional downward deflection and off axis offset of the spring relative to the pin joint. Because of this offset, the spring force is not directed on the center of the pin joint but is slightly lower. When the spring is buckled by the mechanism, the buckling force is slightly above the pin joint. Thus, the load cell is going to be reading some combination of the opposing forces and could easily cause the offset seen in Figure 5.4. The best way to eliminate this issue would be to redesign a the buckling mechanism.

Testing of Spring Combinations:

The next step was to test combinations of springs with different properties. The following three different combinations were measured:

1. High Stiffness vs. Medium Stiffness
2. Low Stiffness vs. High Stiffness
3. Low Stiffness vs. Medium Stiffness

The results from these tests are plotted along with force curve obtained from the model in Figures 5.5 through 5.7. The experimental data is graphed as a dashed line while curve generated by the model is displayed as the solid blue line. These results are consistent with the results from 5.4 and have the same discrepancies and variations from the model that were previously discussed. Although, the data is not perfect these graphs clearly demonstrate the creation of a bi-stable series spring mechanism with variable stiffness.

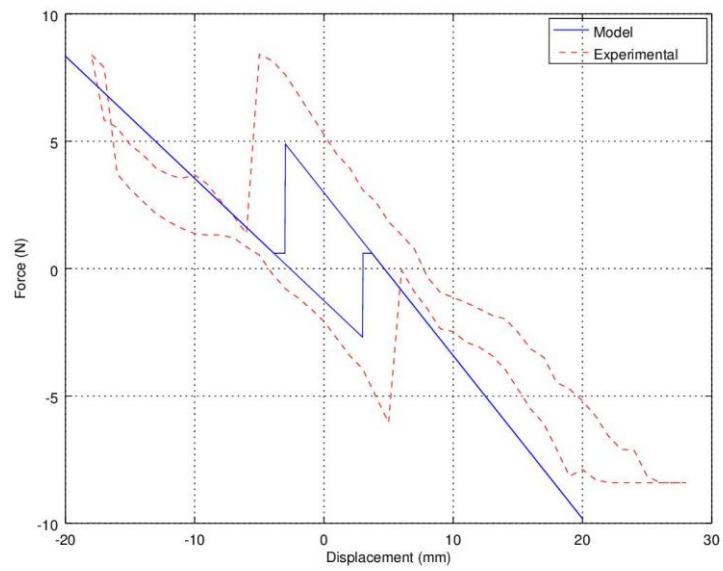


Figure 5.5: High Stiffness Spring A with Medium Stiffness Spring B.

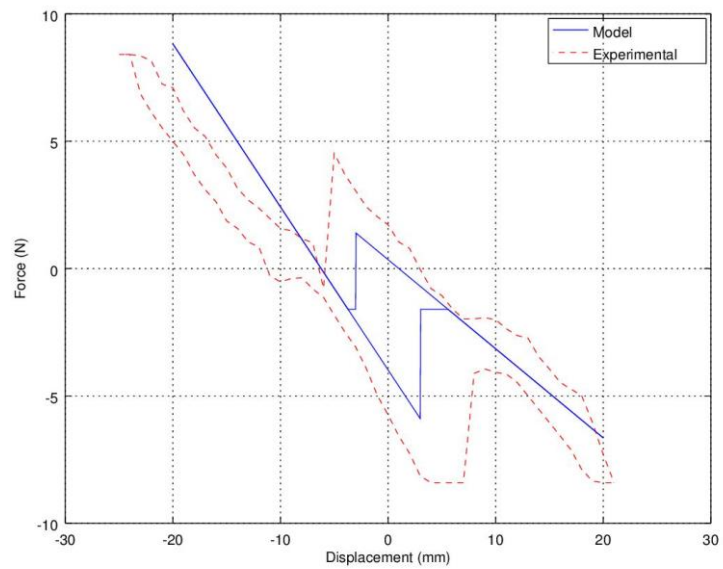


Figure 5.6: Low Stiffness Spring A and High Stiffness Spring B.

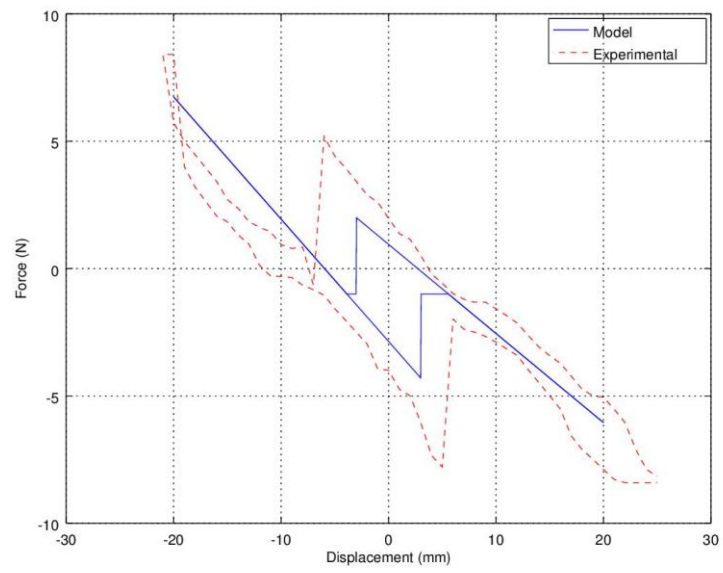


Figure 5.7: Low Stiffness Spring A and Medium Stiffness Spring B.

CHAPTER SIX: CONCLUSION

A method for designing, analyzing, and fabricating a bi-stable, compliant, variable stiffness mechanism has been presented. The simplicity of the series spring design makes it ideal for modeling and scalability. The differences between the experimental data and the model can easily be explained and most likely reflect flaws in the prototype mechanism's design and not in the accuracy of the model. This is most likely caused by a lack of an instantaneous buckling point in the prototype mechanism. In the simulated models, buckling occurs at a predefined position relative to the carriage portion of the device. In the prototype, this buckling point is related to the carriage position through the moment arms and rotational motion of the ends of the spring. Further calibrations to better define the buckling point as a function of the buckling-point adjustment screws is necessary. The model and the experimental data both agree upon the bi-stability and tunable stiffness of the device. As in some of the previous bi-stable mechanisms, the combination of multiple bi-stable mechanism will result in a multi-stable mechanism. However, multi-stable mechanisms generated by the proposed bi-stable devices will result in a different stiffness in each of the configurations. Thus, the proposed work has the ability of generating a new class of soft robotics where each configuration provides the passive tunable compliance.

Future work will include not only automated methods of mechanism optimization but will pursue more compact designs using flexures or cast elastomer members instead of traditional linear springs. Further miniaturization to sub-centimeter scales could result in bulk, tunably-compliant materials for soft robotic devices.

REFERENCES

1. C. Majidi, “Soft robotics: a perspective--current trends and prospects for the future,” *Soft Robot.*, vol. 1, no. 1, pp. 5–11, 2014.
2. G. Tonietti, R. Schiavi, and A. Bicchi, “Design and control of a variable stiffness actuator for safe and fast physical human/robot interaction,” in *Robotics and Automation, 2005. ICRA 2005. Proceedings of the 2005 IEEE International Conference on*, 2005, pp. 526–531.
3. R. Schiavi, G. Grioli, S. Sen, and A. Bicchi, “VSA-II: a novel prototype of variable stiffness actuator for safe and performing robots interacting with humans,” in *Robotics and Automation, 2008. ICRA 2008. IEEE International Conference on*, 2008, pp. 2171–2176.
4. N. G. Tsagarakis, I. Sardellitti, and D. G. Caldwell, “A new variable stiffness actuator (CompAct-VSA): Design and modelling,” in *Intelligent Robots and Systems (IROS), 2011 IEEE/RSJ International Conference on*, 2011, pp. 378–383.
5. N. L. Tagliamonte, F. Sergi, D. Accoto, G. Carpino, and E. Guglielmelli, “Double actuation architectures for rendering variable impedance in compliant robots: A review,” *Mechatronics*, vol. 22, no. 8, pp. 1187–1203, 2012.
6. B. Vanderborght, A. Albu-Schäffer, A. Bicchi, E. Burdet, D. G. Caldwell, R. Carloni, M. Catalano, O. Eiberger, W. Friedl, G. Ganesh, and others, “Variable impedance actuators: A review,” *Rob. Auton. Syst.*, vol. 61, no. 12, pp. 1601–1614, 2013.
7. C. Paul, J. W. Roberts, H. Lipson, and F. J. V. Cuevas, “Gait production in a tensegrity based robot,” in *ICAR’05. Proceedings., 12th International Conference on Advanced Robotics, 2005.*, 2005, pp. 216–222.
8. M. Shibata, F. Saijyo, and S. Hirai, “Crawling by body deformation of tensegrity structure robots,” in *Robotics and Automation, 2009. ICRA’09. IEEE International Conference on*,

2009, pp. 4375–4380.

9. A. Iscen, A. Agogino, V. SunSpiral, and K. Tumer, “Controlling tensegrity robots through evolution,” in *Proceedings of the 15th annual conference on Genetic and evolutionary computation*, 2013, pp. 1293–1300.
10. C. Paul, F. J. Valero-Cuevas, and H. Lipson, “Design and control of tensegrity robots for locomotion,” *IEEE Trans. Robot.*, vol. 22, no. 5, pp. 944–957, 2006.
11. B. D. Jensen, M. B. Parkinson, K. Kurabayashi, L. L. Howell, and M. S. Baker, “ASME International Mechanical Engineering Congress and Exposition, Proceedings,” *2001 ASME International Mechanical Engineering Congress and Exposition*. 2001.
12. J. Qiu, J. H. Lang, and A. H. Slocum, “A Curved-Beam Bistable Mechanism,” *J. Microelectromechanical Syst.*, vol. 13, no. 2, pp. 137–146, Apr. 2004.
13. U. Sönmez and C. C. Tutum, “A Compliant Bistable Mechanism Design Incorporating Elastica Buckling Beam Theory and Pseudo-Rigid-Body Model,” *J. Mech. Des.*, vol. 130, no. 4, p. 42304, 2008.
14. J. Lassoij, N. Tolou, G. Tortora, S. Caccavaro, A. Menciassi, and J. L. Herder, “A statically balanced and bi-stable compliant end effector combined with a laparoscopic 2DoF robotic arm,” *Mech. Sci.*, vol. 3, no. 2, pp. 85–93, Dec. 2012.
15. W. Hartono, “On the Post-buckling Behavior of Elastic Fixed-End Column with Central Brace,” *ZAMM*, vol. 81, no. 9, pp. 605–611, Sep. 2001.
16. S. –R. Li and Y. –H. Zhou, “Post-buckling of a hinged-fixed beam under uniformly distributed follower forces,” *Mech. Res. Commun.*, vol. 32, no. 4, pp. 359–367, 2005.
17. C. Kim and D. Ebenstein, “Curve Decomposition for Large Deflection Analysis of Fixed-Guided Beams With Application to Statically Balanced Compliant Mechanisms,” *J. Mech.*

- Robot.*, vol. 4, no. 4, p. 41009, 2012.
18. T. J. Teo, I.-M. Chen, G. Yang, and W. Lin, “A generic approximation model for analyzing large nonlinear deflection of beam-based flexure joints,” *Precis. Eng.*, vol. 34, no. 3, pp. 607–618, 2010.
 19. B. Todd, B. D. Jensen, S. M. Schultz, and A. R. Hawkins, “Design and Testing of a Thin-Flexure Bistable Mechanism Suitable for Stamping From Metal Sheets,” *J. Mech. Des.*, vol. 132, no. 7, p. 71011, 2010.
 20. G. Chen, Q. T. Aten, S. Zirbel, B. D. Jensen, and L. L. Howell, “A Tristable Mechanism Configuration Employing Orthogonal Compliant Mechanisms,” *J. Mech. Robot.*, vol. 2, no. 1, p. 14501, 2010.